

ARTICLE

DOI: 10.1038/s41467-018-05754-9

OPEN

Atomic engineering of high-density isolated Co atoms on graphene with proximal-atom controlled reaction selectivity

Huan Yan^{1,2}, Xiaoxu Zhao^{2,3}, Na Guo⁴, Zhiyang Lyu², Yonghua Du⁵, Shibo Xi⁵, Rui Guo^{2,6}, Cheng Chen^{2,6}, Zhongxin Chen^{2,3}, Wei Liu², Chuanhao Yao^{1,2}, Jing Li^{1,2}, Stephen J. Pennycook^{3,6,7}, Wei Chen^{2,4,6}, Chenliang Su¹, Chun Zhang^{2,4,6} & Jiong Lu^{1,2,6}

Controllable synthesis of single atom catalysts (SACs) with high loading remains challenging due to the aggregation tendency of metal atoms as the surface coverage increases. Here we report the synthesis of graphene supported cobalt SACs (Co₁/G) with a tuneable high loading by atomic layer deposition. Ozone treatment of the graphene support not only eliminates the undesirable ligands of the pre-deposited metal precursors, but also regenerates active sites for the precise tuning of the density of Co atoms. The Co₁/G SACs also demonstrate exceptional activity and high selectivity for the hydrogenation of nitroarenes to produce azoxy aromatic compounds, attributable to the formation of a coordinatively unsaturated and positively charged catalytically active center (Co–O–C) arising from the proximal-atom induced partial depletion of the 3d Co orbitals. Our findings pave the way for the precise engineering of the metal loading in a variety of SACs for superior catalytic activities.

¹SZU-NUS Collaborative Center and International Collaborative Laboratory of 2D Materials for Optoelectronic Science & Technology, College of Optoelectronic Engineering, Shenzhen University, 518060 Shenzhen, China. ²Department of Chemistry, National University of Singapore, 3 Science Drive 3, Singapore 117543, Singapore. ³NUS Graduate School for Integrative Sciences and Engineering, National University of Singapore, 28 Medical Drive, Singapore 117456, Singapore. ⁴Department of Physics, National University of Singapore, 2 Science Drive 3, Singapore 117542, Singapore. ⁵Institute of Chemical and Engineering Sciences, 1 Pesek Road, Jurong Island, Singapore 627833, Singapore. ⁶Centre for Advanced 2D Materials and Graphene Research Centre, National University of Singapore, 117546, Singapore. ⁷Department of Materials Science & Engineering, National University of Singapore, 9 Engineering Drive 1, Singapore 117575, Singapore. These authors contributed equally: Huan Yan, Xiaoxu Zhao, Na Guo. Correspondence and requests for materials should be addressed to C.S. (email: chmsuc@szu.edu.cn) or to C.Z. (email: phyzc@nus.edu.sg) or to J.L. (email: chmluj@nus.edu.sg)

Single-atom catalysts (SACs) have emerged as a new frontier in the field of heterogeneous catalysis due to their remarkable catalytic performances and maximized atom utilization^{1–21}. For SACs to be practicably applicable, a sufficiently high loading of atomically-dispersed atoms on an appropriate support is required. Unfortunately, isolated metal atoms are thermodynamically unstable due to their high surface energy and thus prone to agglomeration at an increased loading during the synthetic process or the subsequent treatment. Common strategies to tackle this issue include reducing the metal loading to an extremely low level^{1,3,9,22} and enhancing metal-support interactions for a strong anchoring of the isolated metal atoms^{13,23–25}. In respect of the former strategy, the loading of the majority of SACs synthesized by wet-chemistry methods has been kept below 1% to prevent the formation of metal nanoparticles^{1,4,11,22,26,27}. For instance, aggregation of Pt atoms dispersed on α -MoC surface and mesoporous zeolite substrates occurred once the loading of precious metal catalyst was increased to 0.2 and 0.5%, respectively^{11,26}. In the latter strategy which involves a judicious choice of supports, the loading of Pd single atoms can be increased up to 1.5% on modified TiO₂ nanosheets²⁸. In addition, a high loading of SACs has been achieved using a wet-impregnation^{25,29} or high temperature pyrolysis method³⁰. In both methods however, it was challenging to control the loading of metal atoms on the support surface for optimizing the catalytic performance. Despite considerable progress in recent years, controllable synthesis of stable SACs with sufficiently high loading for high performance catalysis remains a major roadblock towards its practical applications.

On the one hand, a strong interaction between anchored metal atoms and neighboring support atoms is essential for achieving stable high-metal-loading SACs^{25,28}. On the other hand, the metal-support interaction results in modification of the electronic properties of anchored metal atoms, which in turn alters the activity and selectivity of SACs^{25,31}. It is therefore of importance to probe the local coordination environment of single metal atoms and their electronic coupling with support atoms in close proximity. Such a study offers a unique opportunity to further optimize the catalytic performance of SACs, which however, remains largely unexplored.

To this end, we have devised a reliable method via the atomic layer deposition (ALD) technique for the preparation of stable high loading Co₁/G SACs, which also allows the precise tuning of the density of isolated Co atoms on the graphene support. In contrast to solution-phase deposition, self-limiting surface reactions (Fig. 1, Supplementary Figure 1) of ALD ensure that each Co precursor molecule is anchored on a single active site of the graphene support^{5,12,15,17}. Interestingly, the active sites on graphene can be re-generated by ozone treatment in the second pulse of each ALD cycle, allowing for the loading of another batch of Co single atoms. As a result, the loading of Co₁ single atoms can be precisely tuned by controlling the number of Co ALD cycles as illustrated in the Fig. 1. In the selective hydrogenation of nitrobenzene, all the Co₁/G SACs prepared show outstanding activity and remarkable selectivity to azoxy compounds. The mechanistic studies show that the electronic coupling of Co atoms with adjacent oxygen atoms results in more positively charged Co₁ catalytic center, which helps to reduce its binding strength to azoxy compounds. Such an electronic coupling between the Co atom and its neighboring oxygen atoms prevents the full hydrogenation of nitroarenes, leading to a remarkably high selectivity towards the partially hydrogenated product.

Results and discussion

Synthesis of Co₁/G SACs. In our study, reduced graphene oxide was selected as the support for the preparation of Co₁/G SACs

due to the following figures of merit: (i) chemically derived graphene offers an ideal low-cost platform for the anchoring of individual Co ALD precursors to the oxygen-decorated carbon sites;³² (ii) the density of anchoring sites on graphene can be tuned by controlling the pretreatment conditions^{32–34}. Under typical oxidation conditions, the basal plane of graphene can be decorated with diverse oxygen functional groups including hydroxyl, epoxy, phenolic, carbonyl, and carboxyl groups³². However, only specific oxygen-containing functional groups on the graphene surface are expected to act as nucleation sites to react with the metal precursors used in the ALD. Hence, it is desirable to achieve homogenous oxidation of graphene to create a high density of identical anchor sites in order to optimize the loading density of Co₁ single atoms. The exposure of graphene to ozone (O₃) at an elevated temperature is most likely to produce uniform epoxy functional groups^{34,35}, which are anticipated to be active anchor sites for Co(C₅H₅)₂ precursors (CoCp₂). Furthermore, the remaining ligands of the deposited metal precursors are often removed through a combustion reaction using O₃ in the second pulse of each ALD cycle³⁶. Hence, we expect the ozonation of a graphene support at elevated temperature to achieve two outcomes, namely allowing us to burn off organic ligands and to recreate desirable anchor sites for the subsequent Co ALD cycles, which would offer an effective method for tuning the metal loading of SACs.

To test the above hypothesis, we performed X-ray photoemission spectroscopy (XPS) measurements to investigate the evolution of the amount of oxygen-containing groups on graphene exposed to O₃ at 150 °C (Supplementary Figure 2). It was found that ozonation of graphene at 150 °C creates predominantly epoxy groups as confirmed by the observation of a strong O1s peak at 532.08 eV, consistent with a previous report³³. The increase in the amount of epoxy groups on the graphene support is approximately linear in the first five cycles of ozone pretreatment but tends to plateau as the number of ozone pretreatment cycles further increases (Fig. 2g). After gaining a better understanding of the ozonation of graphene, we carried out the first cycle of Co ALD on thermally reduced graphene oxide by exposing the support to CoCp₂ vapor as illustrated in Fig. 1. Subsequently, molecular O₃ was injected into the chamber to remove the ligand and to simultaneously recreate new active sites for the loading of another batch of Co atoms in the subsequent cycle of ALD. By repeating this stepwise deposition, the loading density of Co₁/G catalysts can be precisely tuned by controlling the number of Co ALD cycles. Through this method, we managed to synthesize a series of Co₁/G catalysts with Co loadings of 0.4, 0.8, 1.3, 2.0, and 2.5 wt% (designated as Co₁/G-0.4, Co₁/G-0.8, Co₁/G-1.3, Co₁/G-2.0, and Co₁/G-2.5) by performing 1, 2, 3, 4, 5 cycles of Co ALD respectively.

Characterization of Co₁/G SACs. State-of-the-art aberration-corrected scanning transmission electron microscopy – annular dark field (STEM-ADF) measurements were initially conducted to gain a detailed understanding of the morphologies of the as-prepared Co₁/G SACs. The employed acceleration voltage is 60 kV, where the lower voltage significantly reduces the cross section of Co atoms dissociation or clustering events. The large-field-of-view STEM-ADF images of the as-prepared Co₁/G SACs revealed the absence of larger clusters for all the samples prepared within the five cycles of Co ALD as shown in Fig. 1f and Supplementary Figure 3. Compared to the bare graphene (Supplementary Figure 4), atomic resolution STEM-ADF images revealed that Co atoms in Co₁/G-0.4 (Fig. 2a) and Co₁/G-0.8 (Fig. 2b) prepared in the first and second cycle of Co ALD respectively are atomically dispersed and well-separated on graphene without aggregation

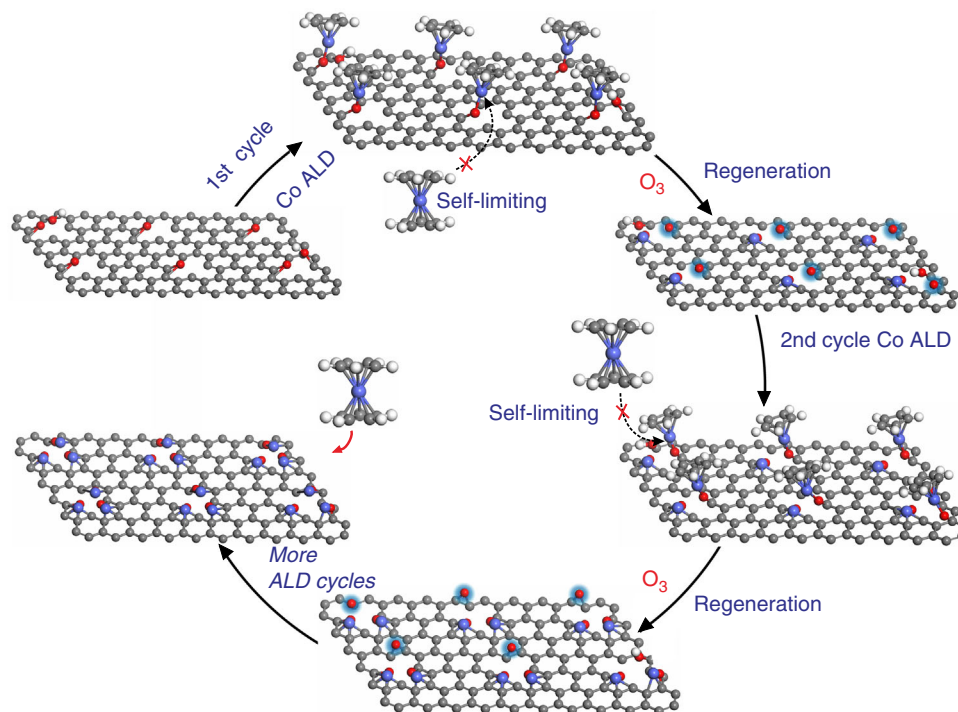


Fig. 1 Schematic illustration of the synthesis of Co_1/G SACs with tuneable loadings. The first cycle of Co ALD by an alternative exposure of the support to CoCp_2 vapor and O_3 gas at 150°C ; the second cycle of Co ALD on Co_1/G to deposit another batch of Co atoms on the active sites created by O_3 treatment at 150°C in the previous Co ALD cycle; more cycles of Co ALD results in a high loading of Co_1 SACs. The balls in gray, white, red, and blue represent carbon, hydrogen, oxygen, and cobalt, respectively

into particles or other Co species (Supplementary Figure 5a–5d and Supplementary Figure 6). The presence of isolated Co atoms was further confirmed by EDS-mapping (Supplementary Figure 5e–g). Interestingly, an increase in the Co loading generated by performing more cycles of Co ALD continued to produce well-dispersed Co single atoms rather than large Co clusters and nanoparticles (Fig. 2c–e, Supplementary Figure 7–9). To our delight, the Co particles or clusters were barely present on graphene even at high loading densities of 2 wt% and 2.5 wt% (Fig. 2d, e, Supplementary Figure 8, 9). We also found that the density of Co single atoms loaded on graphene is closely correlated to the amount of epoxy groups present on the support (Fig. 2g), which further supports the idea that the epoxy groups act as anchor sites for the Co precursors as illustrated in Fig. 1. In order to probe the local chemical environment of Co atoms, we have conducted spatial-dependent electron energy loss spectra (EELS) measurements off (1) and on (2, 3) Co atom sites as marked in the inset of Fig. 2f. In contrast to the featureless curves (green) taken in the bare graphene region, the EELS acquired on single Co atom sites reveal the coexistence of Co $L_{2,3}$ edge and O K edge related peaks, suggesting that the anchoring of isolated Co atoms in graphene involves oxygen atoms. Furthermore, examination of the Co $L_{2,3}$ edge fine structure shows sharp white features with an L_3/L_2 ratio of ~ 5 , suggesting an oxidation state which is lower than +2 valence state³⁷. Such an atomic insight not only provides compelling evidence for the presence of Co–O bonds at the catalytically active sites but also rationalises the proposed atomic structures of Co_1/G SACs as will be discussed in more details later.

The XAFS is a state-of-the-art method to probe the local information of the adsorbing atoms. In our experiment, it was used to investigate the structural and electronic states of the Co_1/G SACs with different loadings. As shown in Fig. 3a, the XANES white line peaks of the Co_1/G SACs samples with different

loadings are centered at 7727.1 eV, between that of the Co foil (7725.7 eV) and Co_3O_4 (7728.0 eV), consistent with the Co_1/G SACs as-prepared being in the oxidized state rather than the metallic state. Additional structural information can also be explicitly inferred from the extended X-ray adsorption fine structure (EXAFS) spectra at the Co K-edge (Fig. 3c and Supplementary Figure 1, 0). Further, the Fourier transform (FT) $k^3\chi(k)$ spectrum of the CoCp_2 molecule exhibits a dominant peak centered at 1.60 Å assignable to the Co–C bonds of the CoCp_2 precursors. In contrast, the EXAFS spectrum (labeled as CoCp/G) acquired on the graphene support after exposure to CoCp_2 vapor at 150°C shows one main peak at 1.58 Å. This suggests the existence of a shorter bond which may result from the chemisorption of CoCp_2 precursors to graphene. As illustrated in Fig. 1, it is naturally expected that CoCp_2 precursors react with the epoxy groups on graphene by removing one of Cp ligands. Hence, the resultant Co atoms will be bonded to one remaining Cp ligand and oxygen atoms on graphene, giving rise to a shorter Co–C/O bond length as compared with that of Co–C bonds in CoCp_2 molecules. In addition, the FT spectra for a series of Co_1/G SACs show that the first shell peaks undergo a further downshift to 1.56 Å as compared to that of CoCp/G , indicating that the bonding of Co on the basal plane of graphene is further strengthened due to the Co atoms forming new chemical bonds with graphene after the complete removal of organic ligands via the O_3 treatment. These observations are consistent with the bonding information extracted from the EXAFS fitting results (Supplementary Table 1). It is also worth noting that the major peaks at 2.18 Å and 2.48 Å of the FT spectra acquired on Co foil and Co_3O_4 respectively are absent in the corresponding spectra of all the Co_1/G SACs, which further confirms that Co atoms remained well dispersed on the graphene support at the high loading of 2.5 wt%, in line with the STEM results.

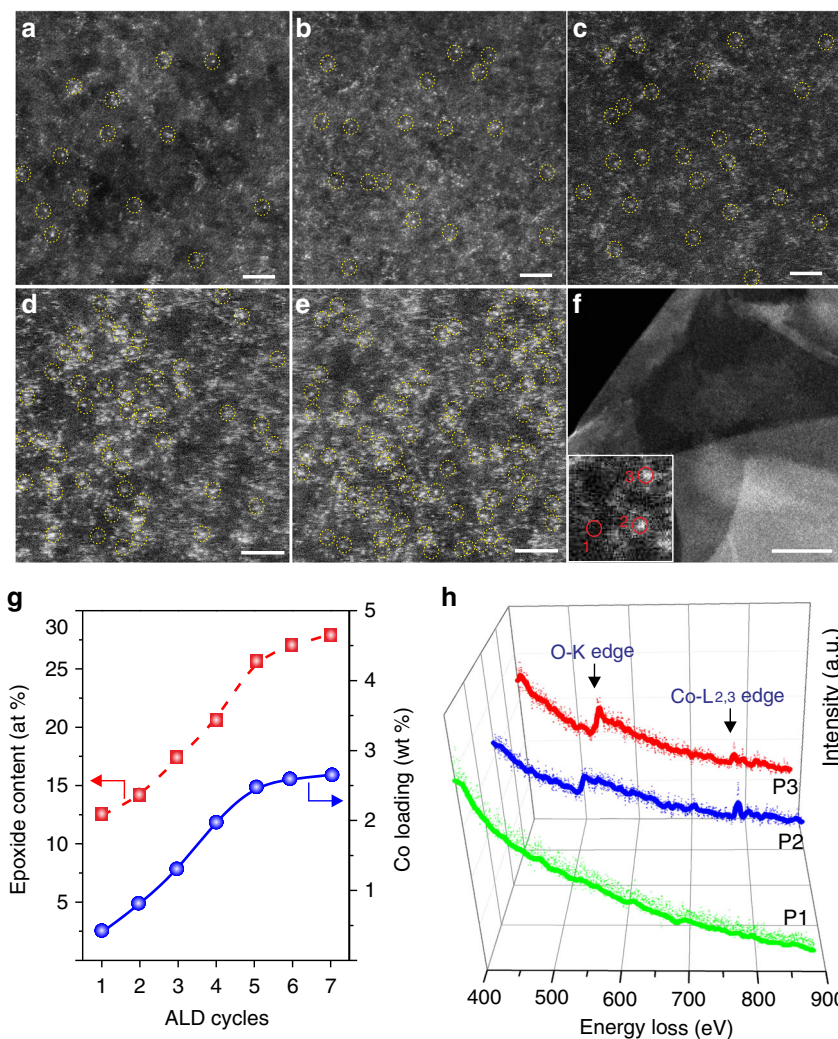


Fig. 2 Structural characterization and identification of Co_1/G SACs. Aberration-corrected STEM-ADF images of Co_1/G -0.4 (**a**), Co_1/G -0.8 (**b**), Co_1/G -1.3 (**c**), Co_1/G -2.0 (**d**), and Co_1/G -2.5 (**e**). Scale bars, 2 nm (**a–e**), 50 nm (**f**). **f** The STEM-ADF image of Co_1/G -2.5 catalysts at low magnification. **g** The evolution of epoxy content in graphene and Co loadings of Co_1/G SACs catalysts as a function of the number of ALD cycles. **h** EEL spectra of O K-edge and Co $L_{2,3}$ -edge acquired in the bare graphene region (position 1 as marked in the inset of **f**) and the isolated Co atom sites (Position 2, 3 as marked in the inset of **f**)

DFT calculations. In order to determine the atomic structures of the Co_1/G SACs, we performed DFT calculations in combination with a standard XAFS fitting method (Supplementary Figure 1, 2-1, 7). Based on the plausible Co ALD reaction mechanism on the defect-rich graphene support (Supplementary Figure 1, 1), it is most likely that the isolated Co atoms are anchored in vacancy related structures through bonding to oxygen species as revealed in our EELS measurements. We hence propose several possible atomic configurations of the Co_1/G SACs along this line (Supplementary Figure 1, 2-1, 3), which are further optimized via DFT calculations. Our calculations reveal a stable structure consisting of CoCp bonded to the graphene support via two interfacial O atoms and one C atom for the CoCp/G sample (Supplementary Figure 1, 2a). Such a structure is expected to be generated in the first step of ALD cycle (Fig. 1), in line with previous work³⁸. After the removal of ligand (Cp), isolated Co atoms in the Co_1/G SACs can be anchored to the divacancy of graphene through bonding with two interfacial O atoms and four C atoms, forming a new structure represented by $\text{Co}_1\text{-O}_2\text{C}_4$ (Supplementary Figure 1, 2b). In order to verify these two structures, we calculated their XANES (Fig. 3b) and fitted their EXAFS (Supplementary Figure 1, 5-1, 7) spectra, which show a good agreement with our experimental

data acquired on CoCp/G and Co_1/G SACs respectively (Fig. 3b, Supplementary Figure 1, 3-1, 7 and Supplement Table 1). In contrast, the calculated XANES spectra of other DFT-modeled structures fail to reproduce the main features of experimental curves (Supplementary Figure 1, 4). Hence, it is most likely the Co_1/G SACs prepared here contains a six-coordinated structure ($\text{Co}_1\text{-O}_2\text{C}_4$), wherein individual Co atoms are bonded to two interfacial O atoms and four C atoms.

Catalytic activity. Azoxybenzene is one of the most important industrial media of the dye and pharmacy industries^{39,40}. The catalytic selective hydrogenation of nitrobenzene has been a major method for the synthesis of azoxybenzene. Unfortunately, the catalysts employed for industrial-scale production of azoxybenzene are usually toxic⁴¹. Noble metal heterogeneous catalysts have recently emerged as promising catalysts for the synthesis of azoxybenzene^{42–44}. However, these catalysts are not practical for the scalable synthesis of azoxybenzene due to their high cost. Here we employ the Co_1/G SACs in the selective hydrogenation of a wide range of substituted nitrobenzene to produce azoxy products as illustrated in Fig. 4a. As shown in Fig. 4b,

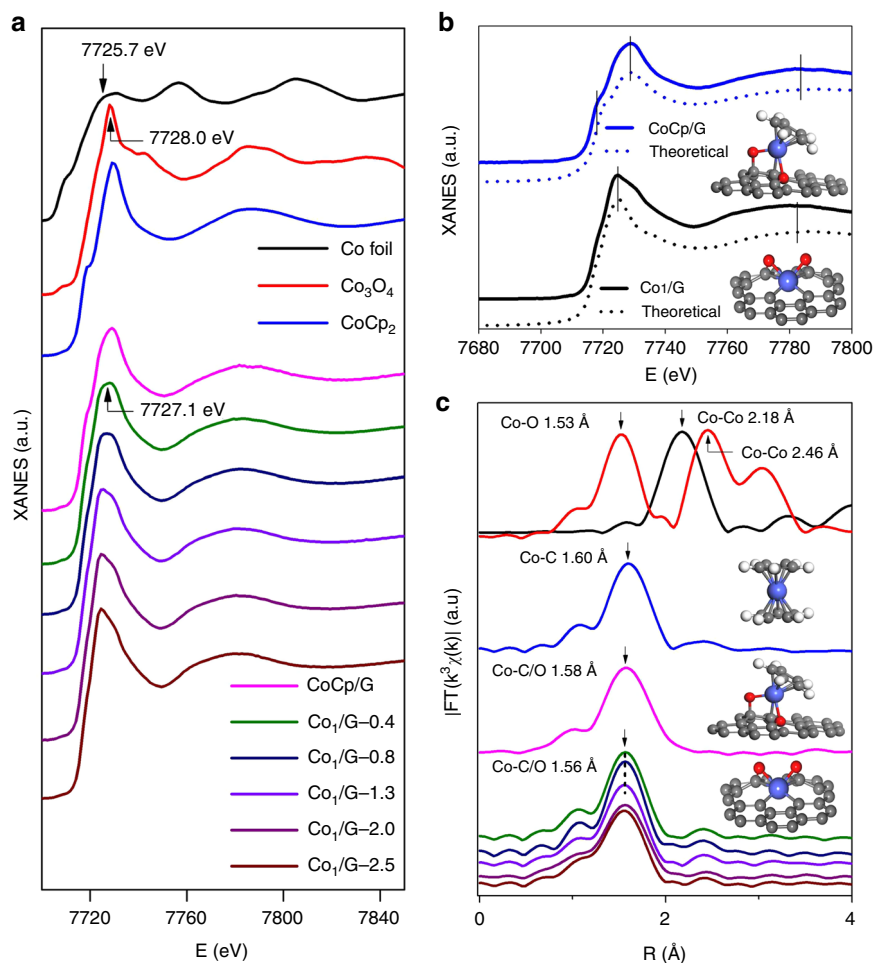


Fig. 3 Co K-edge XAFS and EXAFS spectra of CoCp/G, Co₁/G SACs. **a** Co K-edge XAFS spectra. **b** The experimental XANES curves are compared with the calculated XANES data of optimized DFT-modeled structures of Co₁/G and CoCp/G (inset shows the atomic structures of the models). **c** Fourier transform (FT) extended x-ray absorption fine structure (EXAFS) of these samples with the corresponding structures (insets). The balls in gray, white, red, and blue represent carbon, hydrogen, oxygen, and cobalt, respectively. The Co K-edge XAFS and EXAFS spectra of Co foil, Co₃O₄ and CoCp₂ samples are displayed for comparison. Note: the figure legend in **a** also applies to **c**

all the Co₁/G SACs exhibit much higher selectivity to 3, 3'-dichlorideazoxybenzene (98%), compared to Pt/carbon (18%) and Co-NPs/G (4%) (Supplementary Figure 1, 8-1, 9). For different substituted nitrobenzene (compound 1-6) (Fig. 4c, d and Supplementary Figure 20), all the Co₁/G SACs also exhibit significantly higher selectivity to azoxy compounds (~90%) compared to Pt/carbon (18~21%) and Co-NPs/G (2-3%). The major product over Pt/carbon and Co-NPs/G catalysts is aniline compound, giving rise to a low selectivity to azoxy compounds⁴⁵⁻⁴⁷. In addition, the Co nanoparticles (Supplementary Figure 2, 1) synthesized by ALD (designated as Co-NPs/G-ALD) show a low selectivity (~5%) to azoxy compounds (Supplementary Figure 22). All the azoxybenzene products were verified by their characteristic ¹HNMR and ¹³CNMR spectra (Supplementary Figure 23-36)⁴⁸. Importantly, the Co₁/G SACs with different loadings show negligible variations in the selectivity towards all azoxy compounds (Fig. 4b-d), presumably due to a relatively uniform dispersion of isolated Co atoms for all the Co₁/G SACs catalysts.

The excellent atomic dispersion of all the Co₁/G SACs with different loadings indeed results in a similar turnover frequency (TOF) of 0.33 s⁻¹, which is 6 times higher than that of Co nanoparticles (0.05 s⁻¹) as shown in Fig. 4e. In addition, Co₁/G SACs synthesized exhibit higher catalytic activity and selectivity in the hydrogenation of nitrobenzene as compared to non-noble

metal catalysts reported in the previous work (Supplementary Table 2). Moreover, as shown in Fig. 4e, the TOF of Co₁/G SACs is even higher than that of Pt/carbon (0.23 s⁻¹), which proves their superior catalytic performance comparable to that of precious catalysts. To our delight, Co₁/G SACs with a high loading of 2.5 wt% also exhibit a high durability in the selective hydrogenation of nitroarenes as revealed in the recyclability test (Supplementary Figure 37).

The hydrogenation of nitrobenzene is expected to occur through multiple steps, involving the generation of different reaction intermediates (Supplementary Figure 38)^{49,50}. The adsorption energy of the intermediate compounds on catalytic surface is one of the key factors that determine the selectivity to certain target products⁵¹. In our system, we observed that azoxy compound is the major product when Co₁/G SACs is applied. This indicates that the reaction stops at step 4 (Supplementary Figure 38) is prohibited, preventing the further hydrogenation of azoxy compound to aniline. Such a reasoning is also reported in the previous work⁵². Therefore, we performed DFT calculations of the adsorption energies of azoxybenzene molecules on Co (111), Co₁/G SACs and catalytic centers consisting of isolated Co atoms coordinated to four carbon atoms in a graphene divacancy (labeled as Co₁-C₄/G). It's worth mentioning here that the catalytic activity of graphene-based metal SACs has been

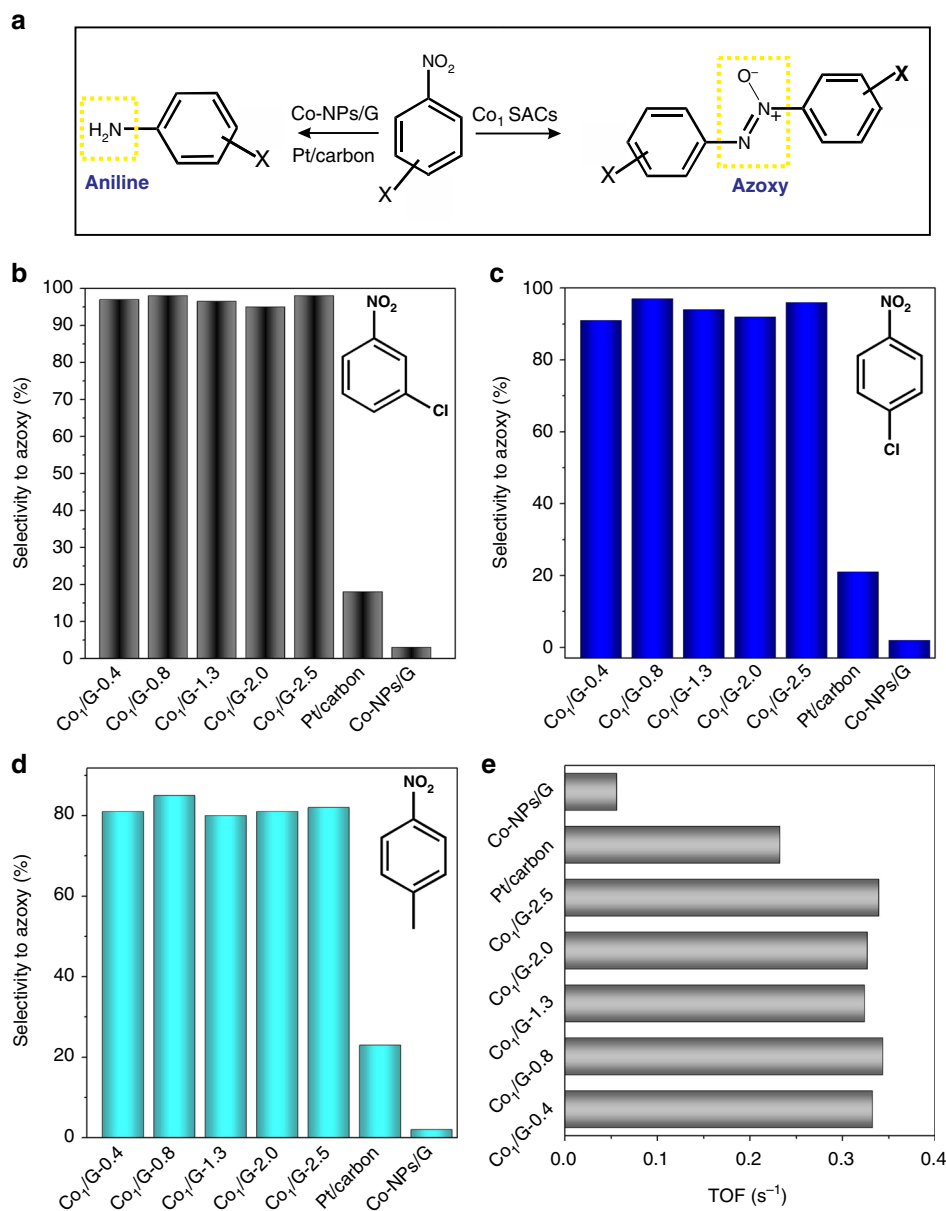


Fig. 4 Catalytic selectivity to azoxy products of various Co_1/G SACs catalysts. **a** Schematic illustration of the hydrogenation of nitroarenes using different catalysts. Histograms of the selectivity to azoxy products for the hydrogenation of 1-chloride-3-nitrobenzene (**b**), 1-chloride-4-nitrobenzene (**c**), and 1-methyl-4-nitrobenzene (**d**) at $\sim 100\%$ conversion of nitroarenes by using different Co_1/G SACs including $\text{Co}_1/\text{G}-0.4$, $\text{Co}_1/\text{G}-0.8$, $\text{Co}_1/\text{G}-1.3$, $\text{Co}_1/\text{G}-2.0$, $\text{Co}_1/\text{G}-2.5$, $\text{Co-NPs}/\text{G}$, and Pt/carbon . **e** Turnover frequency (TOF) of the different catalysts tested in the selective hydrogenation of nitrobenzene

predicted in previous theoretical studies^{53–55}, but catalytic role of atoms proximal to single metal atom remains largely unexplored. Here, we found that holding Co and oxygen atoms in the close proximity is the key that allows the reaction to proceed with extremely high selectivity in the partial hydrogenation of nitrobenzene to azoxybenzene. Such an excellent catalytic performance can be attributed to the different binding nature of the reactants adsorbed at different catalytic sites. As shown in the Fig. 5a, the dispersion-corrected DFT (DFT-D2) calculations revealed that azoxybenzene shows a stand-up adsorption geometry on Co (111) with a large adsorption energy of -1.15 eV. In the case of the $\text{Co}_1\text{-C}_4/\text{G}$, the azoxybenzene exhibits a flat adsorption geometry over the $\text{Co}_1\text{-C}_4$ site with an even larger adsorption energy of -1.55 eV (Fig. 5a). In contrast, the azoxybenzene binds to the $\text{Co}_1\text{-O}_2\text{C}_4$ site of Co_1/G SACs weakly with a small adsorption energy of 0.52 eV. In addition, the

separation between azoxybenzene and the Co catalytic center becomes larger for the weak adsorption case (Co_1/G SACs) (Supplementary Figure 39). Furthermore, it is observed that the charge redistribution at the interface in the cases of Co (111) and $\text{Co}_1\text{-C}_4/\text{G}$ is more significant than that of azoxybenzene adsorbed on the $\text{Co-O}_2\text{C}_4$ site of Co_1/G SACs (Supplementary Figure 40a–c). The weak adsorption of azoxy compounds over Co_1/G SACs might be insufficient to break the N–O bond of azoxybenzene for further hydrogenation, giving rise to a high selectivity to azoxybenzene (Supplementary Figure 40d)^{49,52}.

To gain more insights into the catalytic role of proximal atoms in the SACs, we also calculated the projected density of states (PDOS) of the Co atom to d and s orbitals for both Co_1/G and $\text{Co}_1\text{-C}_4/\text{G}$ (a hypothetical structure without proximal oxygen atom for a comparison). As shown in Fig. 5b, the PDOS of Co 3d orbitals around Fermi energy (E_F) is dramatically different in the

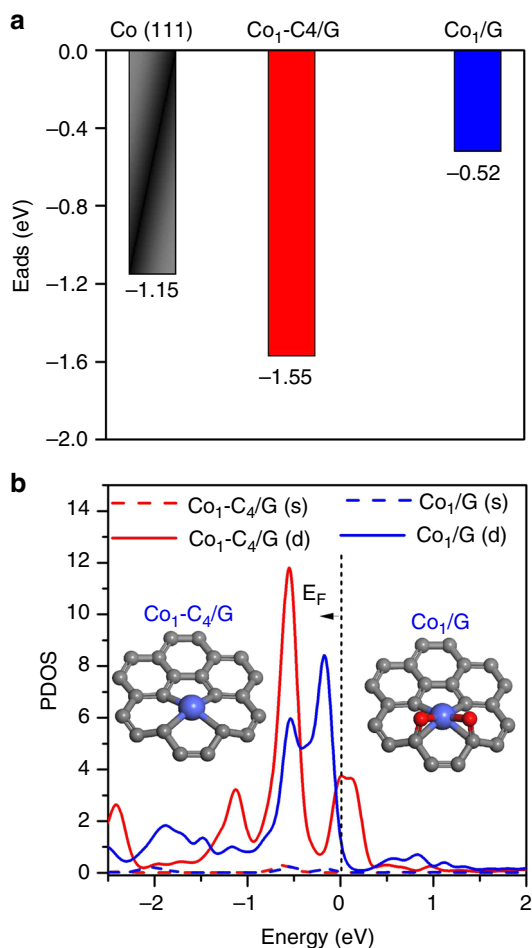


Fig. 5 Theoretical simulations of the catalytic origins. **a** Adsorption energies for the azoxybenzene on Co (111) facet, Co₁-C₄/G and Co₁/G SACs. **b** The partial density of state (PDOS) projected on the Co 4s and 3d orbitals of Co₁-C₄/G and Co₁/G. The balls in gray, red, and blue represent carbon, oxygen, and cobalt, respectively

two examined structures while the difference for PDOS of Co 4s orbitals is much less significant. The PDOS of Co 3d of Co₁-C₄/G exhibit a noticeable peak at E_F contributed by the partially filled *d* orbitals. In contrast, the presence of oxygen atoms proximal to Co₁ in Co₁/G SACs pushes these partially filled *d* orbitals above E_F, resulting in a lower PDOS at E_F and thus a more positively charged Co atom. Consistently, Bader charge transfer analysis⁵⁶ also reveals that each Co atom in Co₁/G SACs loses more electrons (~0.8 electrons) to the surrounding O and C atoms compared to Co atoms in Co₁-C₄/G (lose 0.65 electrons to the surrounding atoms). A more positively charged Co₁-O₂C₄ active center disfavors the adsorption of electron-deficient azoxybenzene on the Co₁-O₂C₄ of Co₁/G SACs for the further hydrogenation to azobenzene, which in turn leads to a higher selectivity towards azoxybenzene (Supplementary Figure 40d)^{51,57}. The excellent catalytic performance of Co₁/G SACs discovered in our study attests to their great potential in a wide range of selective hydrogenation reactions.

In conclusion, we have developed a stepwise approach to fabricate a series of Co₁/G SACs with high and precisely tunable loadings. Our results reveal that the ozone treatment of a graphene support at mild ALD conditions not only burns off metal ligands, but also recreates active sites for the subsequent anchoring of another batch of Co atoms. This unique approach allows us to precisely tune the density of the supported Co atoms from 0.4% up to 2.5% without formation of any Co nanoparticle

or clusters. As compared to conventional Co nanoparticles and precious Pt/carbon catalysts, all the Co₁/G SACs exhibit remarkably high selectivity towards azoxy compounds in the hydrogenation of nitrobenzene aromatics. This can be attributed to the electronic coupling between Co atoms and adjacent oxygen atoms that results in a positively charged catalytic center. Consequently, the adsorption of electron deficient azoxy compounds is weaker and thus the full hydrogenation of nitroarenes is prevented. Our findings have opened up an unprecedented avenue to precisely control the loading of single metal atoms in a wide range of SACs for industrially important chemical transformations.

Methods

Materials. All the chemicals were purchased from Sigma Aldrich and were used as received without further purification. These includes Bis (cyclopentadienyl) cobalt (CoCp₂, 98%), Co(NO₃)₂·6H₂O (98%, trace metals basis), the Pt/carbon catalyst, sodium borohydride (99.99%, trace metals basis) and all the substituted nitrobenzenes. Few-layer graphene oxide and pristine graphene nanosheet (99.5%) were purchased from Nanjing XFNANO Materials Tech Co. Ltd. and Chengdu Organic Chemicals Co. Ltd., Chinese Academy of Sciences respectively.

Synthesis of Co₁/G SACs. The synthesis of Co₁ SACs was performed in a viscous ALD flow reactor (Plasma-assisted ALD system, Wuxi MNT Micro and Nanotech Co., Ltd, China) by alternatively exposing thermally-reduced graphene oxide to CoCp₂ precursor and O₃ at 150 °C. Ultrahigh purity N₂ (99.99%) was used as carrier gas with a flow rate of 50 mL/min. The Co precursor was heated at 100 °C to generate a high enough vapor pressure. The reactor and reactor inlets were held at 150 °C and 120 °C respectively to avoid any precursor condensation. An in-situ thermal reduction of as-received graphene oxide support was conducted at 300 °C for 5 min before performing Co ALD. The timing sequence was 100, 120, 150, and 120 seconds for the CoCp₂ exposure, N₂ purge, O₃ exposure and N₂ purge, respectively. Conducting Co ALD with 1, 2, 3, 4 and 5 cycles allows for the synthesis of Co₁/G-0.4, Co₁/G-0.8, Co₁/G-1.3, Co₁/G-2.0, and Co₁/G-2.5, respectively.

Synthesis of Co-NPs/G. The Co-NPs/G was synthesized using the previous method⁵⁸. In brief, 100 mg of the graphene oxide was dispersed in 15 mL of ethanol with sonication. Meanwhile, 10 mg of Co(NO₃)₂·6H₂O (1 mmol) was added into 15 mL of ultrapure water. After that, NaOH solution (6 M) was added into as-prepared Co(NO₃)₂ solution. Co(OH)₂ precipitated was filtered and washed multiple times using ultrapure water and ethanol. The Co(OH)₂ solid was then dispersed into ethanol with sonication, and gradually added into graphene oxide dispersion followed by a continuous stirring for 1 h. In order to keep the pH at 11, 6 M NaOH solution was used during the synthesis. Then, 1 ml of N₂H₄·H₂O was added and stirred for another 30 min. The obtained mixture was put into Teflon-lined stainless autoclave at 180 °C for 12 h. The sample was dried at 60 °C after filtration and washing. Before used in the catalytic reaction, as-prepared samples were calcined at 150 °C in air, and reduced under a flow of 10% H₂/Ar gas at 150 °C.

The characterization of as-prepared catalysts. The Co loadings in all the samples were measured by an inductively coupled plasma atomic emission spectrometer (ICP-AES); therein all samples were dissolved in hot fresh aqua regia. XPS measurements were carried out in a custom-designed ultrahigh vacuum (UHV) system with a base pressure better than 2 × 10⁻¹⁰ mbar. Al Kα (hν = 1486.7 eV) was used as the excitation sources for XPS. ¹H and ¹³C NMR spectra were recorded on a Bruker AV 300 (300 MHz) and Bruker AV500 (500 MHz) spectrometer. Chemical shifts were reported in parts per million (ppm), and the residual solvent peak was used as an internal reference: ¹H (chloroform δ 7.27), ¹³C (chloroform δ 77.0).

STEM-ADF characterization and image simulation: STEM-ADF imaging was carried out in an aberration-corrected JEOL ARM-200F system equipped with a cold field emission gun and an ASCOR probe corrector at 60 kV. The images were collected with a half-angle range from ~85 to 280 mrad, and the convergence semiangle was set at ~30 mrad. The imaging dose rate for single frame imaging is estimated as 8 × 10⁵ e/nm²·s with a total dose of 1.6 × 10⁷ e/nm². The dwell time for STEM-ADF image is set as 20 us/pixel. The EELS 2D maps were taken by Gatan Quantum ER Spectrometer with a spectrum pixel size of 2 s.

The X-ray absorption near edge structure (XANES) and the extended X-ray absorption fine structure (EXAFS) measurements of Co K-edge were carried out at the XAFCA beamline of the Singapore Synchrotron Light Source (SSLS)⁵⁹. The storage ring of SSLS operated at 700 MeV with beam current of 250 mA. A Si (111) double-crystal monochromator was applied to filter the X-ray beam. Co foils were used for the energy calibration, and all samples were measured under transmission

mode at room temperature. The EXAFS oscillations $\chi(k)$ were extracted and analyzed using the Demeter software package⁶⁰.

DFT calculations. The first-principles calculations are performed with density functional theory (DFT) by utilizing the Vienna ab-initio Simulation Package (VASP)⁶¹. The generalized gradient approximation (GGA) in the Perdew-Burke-Ernzerh (PBE) format^{62,63} and the projector-augmented wave (PAW) method⁶⁴ are employed in all calculations. A plane wave basis with a cut-off energy of 450 eV along with spin polarization and $4 \times 4 \times 1$ k-sampling in Brillouin zone are used for all calculations. The convergence criterion for structural relaxations is set to 0.01 eV/Å. Effects of Van der Waals force (through DFT + D2)⁶⁵ are also considered. Defective graphene is defined with an 8×8 unit cell with a divacancy consisting of two missing adjacent C atoms (Figure S5). The Co (111) surface is described with a 4×4 unit cell with 5 atomic layers. The Co atoms of the bottom three layers are kept fixed in the relaxation process. 18 Å of a vacuum layer in perpendicular direction is included into supercells to avoid unphysical interactions between neighboring unit cells.

XANES simulations. The XANES spectra of Co K edges of all the structures predicted by DFT were modeled using a finite difference method implemented by FDMNES program⁶⁶. For the FDMNES calculation, the Schrödinger equation is solved with a free shape of potential, which avoids using the muffin-tin approximation and thus better reproduce the theoretical XANES spectrum. For all the calculated XANESs, the final states are calculated inside a sphere with a size of 8 Å. The energy step at the Fermi level is 0.2 eV.

Hydrogenation of nitrobenzene and its derivatives. 0.1 mmol of substrates, 1.4×10^{-3} mmol of catalyst, 2 mmol sodium borohydride, 8 mL of Tetrahydrofuran (THF) and 2 ml of ultrapure water were mixed in a round-bottom flask to carry out the reaction. Then the reaction mixture was stirred at 25 °C for one hour. The as-obtained products were analyzed by GC-MS (7890 A GC system, 5975 C inert MSD with Triple-Axis Detector, Agilent Technologies).

Data availability. The data that support the findings of this study are available from the corresponding author upon reasonable request.

Received: 5 January 2018 Accepted: 3 July 2018

Published online: 23 August 2018

References

- Qiao, B. T. et al. Single-atom catalysis of CO oxidation using Pt-1/FeOx. *Nat. Chem.* **3**, 634–641 (2011).
- Kyriakou, G. et al. Isolated metal atom geometries as a strategy for selective heterogeneous hydrogenations. *Science* **335**, 1209–1212 (2012).
- Lin, J. et al. Remarkable performance of Ir-1/FeOx single-atom catalyst in water gas shift reaction. *J. Am. Chem. Soc.* **135**, 15314–15317 (2013).
- Moses-DeBusk, M. et al. CO oxidation on supported single Pt atoms: experimental and ab initio density functional studies of CO interaction with Pt atom on theta-Al₂O₃(010) Surface. *J. Am. Chem. Soc.* **135**, 12634–12645 (2013).
- Sun, S. H. et al. Single-atom catalysis using Pt/graphene achieved through atomic layer deposition. *Sci. Rep.* **3**, 1775 (2013).
- Yang, M., Allard, L. F. & Flytzani-Stephanopoulos, M. Atomically dispersed Au-(OH)(x) species bound on titania catalyze the low-temperature water-gas shift reaction. *J. Am. Chem. Soc.* **135**, 3768–3771 (2013).
- Yang, X. F. et al. Single-atom catalysts: a new frontier in heterogeneous catalysis. *Acc. Chem. Res.* **46**, 1740–1748 (2013).
- Guo, X. et al. Direct, nonoxidative conversion of methane to ethylene, aromatics, and hydrogen. *Science* **344**, 616–619 (2014).
- Wei, H. et al. FeOx-supported platinum single-atom and pseudo-single-atom catalysts for chemoselective hydrogenation of functionalized nitroarenes. *Nat. Commun.* **5**, 5634 (2014).
- Yang, M. et al. Catalytically active Au-O (OH) x-species stabilized by alkali ions on zeolites and mesoporous oxides. *Science* **346**, 1498–1501 (2014).
- Ding, K. et al. Identification of active sites in CO oxidation and water-gas shift over supported Pt catalysts. *Science* **350**, 189–192 (2015).
- Yan, H. et al. Single-atom Pd1/graphene catalyst achieved by atomic layer deposition: remarkable performance in selective hydrogenation of 1, 3-butadiene. *J. Am. Chem. Soc.* **137**, 10484–10487 (2015).
- Jones, J. et al. Thermally stable single-atom platinum-on-ceria catalysts via atom trapping. *Science* **353**, 150–154 (2016).
- Lang, R. et al. Hydroformylation of olefins by a rhodium single-atom catalyst with activity comparable to RhCl (PPh₃)₃. *Angew. Chem. Int. Ed.* **128**, 16288–16292 (2016).
- Cheng, N. et al. Platinum single-atom and cluster catalysis of the hydrogen evolution reaction. *Nat. Commun.* **7**, 13638 (2016).
- Chung, H. T. et al. Direct atomic-level insight into the active sites of a high-performance PGM-free ORR catalyst. *Science* **357**, 479–484 (2017).
- Yan, H. et al. Bottom-up precise synthesis of stable platinum dimers on graphene. *Nat. Commun.* **8**, 1070 (2017).
- Guo, J. et al. Ultrasmall tungsten carbide catalysts stabilized in graphitic layers for high-performance oxygen reduction reaction. *Nano Energy* **28**, 261–268 (2016).
- Wang, H. et al. Platinum-modulated cobalt nanocatalysts for low-temperature aqueous-phase Fischer–Tropsch synthesis. *J. Am. Chem. Soc.* **135**, 4149–4158 (2013).
- Zhang, X. et al. Catalytically active single-atom niobium in graphitic layers. *Nat. Commun.* **4**, 1924 (2013).
- Li, Y. et al. An oxygen reduction electrocatalyst based on carbon nanotube-graphene complexes. *Nat. Nanotechnol.* **7**, 394–400 (2012).
- Vile, G. et al. A stable single-site palladium catalyst for hydrogenations. *Angew. Chem. Int. Ed.* **54**, 11265–11269 (2015).
- Zhang, S. R. et al. WGS catalysis and in situ studies of CoO_{1-x}, PtCo_n/Co₃O₄, and Pt_mCo_n/CoO_{1-x} nanorod catalysts. *J. Am. Chem. Soc.* **135**, 8283–8293 (2013).
- Zhang, S. et al. Catalysis on singly dispersed bimetallic sites. *Nat. Commun.* **6**, 7938 (2015).
- Choi, C. H. et al. Tuning selectivity of electrochemical reactions by atomically dispersed platinum catalyst. *Nat. Commun.* **7**, 10922 (2016).
- Lin, L. et al. Low-temperature hydrogen production from water and methanol using Pt/α-MoC catalysts. *Nature* **544**, 80–83 (2017).
- Zhang, B. et al. Stabilizing a platinum single-atom catalyst on supported phosphomolybdic acid without compromising hydrogenation activity. *Angew. Chem. Int. Ed.* **55**, 8319–8323 (2016).
- Liu, P. X. et al. Photochemical route for synthesizing atomically dispersed palladium catalysts. *Science* **352**, 797–801 (2016).
- Liu, G. et al. MoS₂ monolayer catalyst doped with isolated Co atoms for the hydrodeoxygenation reaction. *Nat. Chem.* **9**, 810–816 (2017).
- Liu, W. et al. Single-atom dispersed Co–N–C catalyst: structure identification and performance for hydrogenative coupling of nitroarenes. *Chem. Sci.* **7**, 5758–5764 (2016).
- Wang, X. et al. Uncoordinated amine groups of metal–organic frameworks to anchor single Ru sites as chemoselective catalysts toward the hydrogenation of quinoline. *J. Am. Chem. Soc.* **139**, 9419–9422 (2017).
- Dreyer, D. R., Park, S., Bielawski, C. W. & Ruoff, R. S. The chemistry of graphene oxide. *Chem. Soc. Rev.* **39**, 228–240 (2010).
- Ganguly, A., Sharma, S., Papakonstantinou, P. & Hamilton, J. Probing the thermal deoxygenation of graphene oxide using high-resolution in situ X-ray-based spectroscopies. *J. Phys. Chem. C* **115**, 17009–17019 (2011).
- Mulyana, Y., Uenuma, M., Ishikawa, Y. & Uraoka, Y. Reversible oxidation of graphene through ultraviolet/ozone treatment and its nonthermal reduction through ultraviolet irradiation. *J. Phys. Chem. C* **118**, 27372–27381 (2014).
- Gao, W. et al. Ozonated graphene oxide film as a proton-exchange membrane. *Angew. Chem. Int. Ed.* **53**, 3588–3593 (2014).
- Chong, Y. T., Yau, E. M. Y., Nielsch, K. & Bachmann, J. Direct atomic layer deposition of ternary ferrites with various magnetic properties. *Chem. Mater.* **22**, 6506–6508 (2010).
- Zhao, Y., Feltes, T. E., Regalbutto, J. R., Meyer, R. J. & Klie, R. F. In situ electron energy loss spectroscopy study of metallic Co and Co oxides. *J. Appl. Phys.* **108**, 063704 (2010).
- Cao, Y. et al. Atomic insight into optimizing hydrogen evolution pathway over a Co₁-N₄ single-site photocatalyst. *Angew. Chem. Int. Ed.* **56**, 12191–12196 (2017).
- Hoult, J. Pharmacological and biochemical actions of sulphasalazine. *Drugs* **32**, 18–26 (1986).
- Waghmode, S. B., Sabne, S. M. & Sivasanker, S. Liquid phase oxidation of amines to azoxy compounds over ETS-10 molecular sieves. *Green. Chem.* **3**, 285–288 (2001).
- Nokubi, T., Kindt, S., Clark, T., Kamimura, A. & Heinrich, M. R. Synthesis of dibenzo [c, e][1, 2] diazocines—a new group of eight-membered cyclic azo compounds. *Tetrahedron Lett.* **56**, 316–320 (2015).
- Corma, A. & Serna, P. Chemoselective hydrogenation of nitro compounds with supported gold catalysts. *Science* **313**, 332–334 (2006).
- Liu, X. et al. Gold-catalyzed direct hydrogenative coupling of nitroarenes to synthesize aromatic azo compounds. *Angew. Chem. Int. Ed.* **53**, 7624–7628 (2014).
- Li, H.-Q. et al. Deoxygenative coupling of nitroarenes for the synthesis of aromatic azo compounds with CO using supported gold catalysts. *Chem. Commun.* **51**, 11217–11220 (2015).
- Zhao, F., Ikushima, Y. & Arai, M. Hydrogenation of nitrobenzene with supported platinum catalysts in supercritical carbon dioxide: effects of pressure, solvent, and metal particle size. *J. Catal.* **224**, 479–483 (2004).

46. Sun, Z. et al. The solvent-free selective hydrogenation of nitrobenzene to aniline: an unexpected catalytic activity of ultrafine Pt nanoparticles deposited on carbon nanotubes. *Green Chem.* **12**, 1007–1011 (2010).
47. Xu, R., Xie, T., Zhao, Y. & Li, Y. Quasi-homogeneous catalytic hydrogenation over monodisperse nickel and cobalt nanoparticles. *Nanotechnology* **18**, 055602 (2007).
48. Hwu, J. R., Das, A. R., Yang, C. W., Huang, J.-J. & Hsu, M.-H. 1, 2-Eliminations in a novel reductive coupling of nitroarenes to give azoxy arenes by sodium bis(trimethylsilyl) amide. *Org. Lett.* **7**, 3211–3214 (2005).
49. Zhu, H., Ke, X., Yang, X., Sarina, S. & Liu, H. Reduction of nitroaromatic compounds on supported gold nanoparticles by visible and ultraviolet light. *Angew. Chem.* **122**, 9851–9855 (2010).
50. Hu, L. et al. Highly efficient synthesis of aromatic azos catalyzed by unsupported ultra-thin Pt nanowires. *Chem. Commun.* **48**, 3445–3447 (2012).
51. Chen, G. et al. Interfacial electronic effects control the reaction selectivity of platinum catalysts. *Nat. Mater.* **15**, 564 (2016).
52. Xiao, Q., Liu, Z., Wang, F., Sarina, S. & Zhu, H. Tuning the reduction power of visible-light photocatalysts of gold nanoparticles for selective reduction of nitroaromatics to azoxy-compounds—Tailoring the catalyst support. *Appl. Catal. B Environ.* **209**, 69–79 (2017).
53. Lu, Y.-H., Zhou, M., Zhang, C. & Feng, Y.-P. Metal-embedded graphene: a possible catalyst with high activity. *J. Phys. Chem. C* **113**, 20156–20160 (2009).
54. Zhou, M., Lu, Y.-H., Cai, Y.-Q., Zhang, C. & Feng, Y.-P. Adsorption of gas molecules on transition metal embedded graphene: a search for high-performance graphene-based catalysts and gas sensors. *Nanotechnology* **22**, 385502 (2011).
55. Guo, N., Xi, Y., Liu, S. & Zhang, C. Greatly enhancing catalytic activity of graphene by doping the underlying metal substrate. *Sci. Rep.* **5**, 12058 (2015).
56. Sanville, E., Kenny, S. D., Smith, R. & Henkelman, G. Improved grid-based algorithm for Bader charge allocation. *J. Comput. Chem.* **28**, 899–908 (2007).
57. Ke, X. et al. Tuning the reduction power of supported gold nanoparticle photocatalysts for selective reductions by manipulating the wavelength of visible light irradiation. *Chem. Commun.* **48**, 3509–3511 (2012).
58. Xu, T., Xue, J., Zhang, X., He, G. & Chen, H. Ultrafine cobalt nanoparticles supported on reduced graphene oxide: efficient catalyst for fast reduction of hexavalent chromium at room temperature. *Appl. Surf. Sci.* **402**, 294–300 (2017).
59. Du, Y. et al. XAFCA: a new XAFS beamline for catalysis research. *J. Synchrotron Radiat.* **22**, 839–843 (2015).
60. Ravel, B. & Newville, M. ATHENA, ARTEMIS, HEPHAESTUS: data analysis for X-ray absorption spectroscopy using IFEFFIT. *J. Synchrotron Radiat.* **12**, 537–541 (2005).
61. Kresse, G. & Hafner, J. Ab initio molecular dynamics for liquid metals. *Phys. Rev. B* **47**, 558 (1993).
62. Kresse, G. & Furthmüller, J. Efficient iterative schemes for ab initio total-energy calculations using a plane-wave basis set. *Phys. Rev. B* **54**, 11169 (1996).
63. Perdew, J. P. et al. Atoms, molecules, solids, and surfaces: applications of the generalized gradient approximation for exchange and correlation. *Phys. Rev. B* **46**, 6671 (1992).
64. Blöchl, P. E. Projector augmented-wave method. *Phys. Rev. B* **50**, 17953 (1994).
65. Grimme, S. Semiempirical GGA-type density functional constructed with a long-range dispersion correction. *J. Comput. Chem.* **27**, 1787–1799 (2006).
66. Bunău, O., & Joly, Y. Self-consistent aspects of x-ray absorption calculations. *J. Phys. Condens. Matter* **21**, 345501 (2009).

Acknowledgements

J. Lu acknowledges the support from NUS start-up grant (R-143-000-621-133) and Tier 1 (R-143-000-637-112) and MOE Tier 2 grant (R-143-000-A06-112). W. Chen acknowledges NSFC grant 91645102. C. Su acknowledges NNSFC (51502174) and Shenzhen Peacock Plan (Grant No. 827-000113, KQTD2016053112042971). C. Zhang acknowledges the support from Singapore National Research Foundation (NRF-CRP13-2014-03 and NRF-CRP16-2015-02). H. Yan appreciates the funding support from the China Postdoctoral Science Foundation (2017M610541).

Author contributions

J.L. supervised the project. H.Y. and J.L. conceived and designed the experiment. H.Y. prepared the catalysts and performed the activity test with the supervision of C.S. and J.L.; X.Z. performed the STEM-ADF and EELS characterization with the supervision of S.J. P.; N.G. performed the theoretical calculation under the supervision of C.Z.; Y.D. and S. X. helped to perform the XAFS measurement. Z.L. helped to establish the ALD system under the supervision of W.C.; R.G. performed the XPS measurements under the supervision of W.C.; C.C. helped to perform the TEM characterization. Z.C., W.L., C.Y., and J.L. assisted in the activity test. H.Y., C.S., C.Z., and J.L. wrote the manuscript. All authors reviewed and contributed to the manuscript.

Additional information

Supplementary Information accompanies this paper at <https://doi.org/10.1038/s41467-018-05754-9>.

Competing interests: The authors declare no competing interests.

Reprints and permission information is available online at <http://npg.nature.com/reprintsandpermissions/>

Publisher's note: Springer Nature remains neutral with regard to jurisdictional claims in published maps and institutional affiliations.



Open Access This article is licensed under a Creative Commons Attribution 4.0 International License, which permits use, sharing, adaptation, distribution and reproduction in any medium or format, as long as you give appropriate credit to the original author(s) and the source, provide a link to the Creative Commons license, and indicate if changes were made. The images or other third party material in this article are included in the article's Creative Commons license, unless indicated otherwise in a credit line to the material. If material is not included in the article's Creative Commons license and your intended use is not permitted by statutory regulation or exceeds the permitted use, you will need to obtain permission directly from the copyright holder. To view a copy of this license, visit <http://creativecommons.org/licenses/by/4.0/>.

© The Author(s) 2018